Full Paper

Journal of the Brazilian Chemical Society

https://dx.doi.org/10.21577/0103-5053.20260096

J. Braz. Chem. Soc. **2026**, *37-Spe2*, e-20260096, 1-8

Hemiaminal Sequestration Enables Organocatalytic [3 + 2] Cycloaddition of Nitrones to Propargylic Aldehydes

Matthijs A. Hellinghuizen,[a] *Aleksandr Y. Pereverzev*[a] *and Jana Roithová*[*,a]

[a]*Institute for Molecules and Materials, Radboud University, Heyendaalseweg 135, 6525AJ Nijmegen, The Netherlands*

The prolinol derivatives are among the most prominent catalysts in aminocatalysis. The installation of silyl ether groups onto the hydroxyl group prevented off-cycle equilibria between iminium intermediates and hemiaminal species, leading to high activity and widespread adoption of these catalysts. However, in the organocatalyzed [3 + 2] cycloaddition of nitrones to propargylic aldehydes, the silyl-protected catalysts proved ineffective, whereas the unprotected catalysts afforded high yields. In this study, this seemingly paradoxical reactivity has been explained using a combination of nuclear magnetic resonance, electrospray ionization mass spectrometry, and infrared photodissociation spectroscopy. Contrary to other reactions, the hemiaminal formation is essential, as it keeps the concentration of free prolinol catalyst in the solution minimal, and thereby hinders the undesired prolinol addition to the iminium intermediate. In the case of silylated catalysts, no hemiaminal can form, and the catalyst is rapidly incorporated into the side product, halting the reaction.

Keywords: mass spectrometry, organic chemistry, methodology and reactions, organocatalysis, reaction mechanism, spectroscopy, spectroscopic properties

Introduction

The advent of organocatalysis has greatly broadened the pool of enantioselective reactions. Reactions previously limited to metal-organic catalysis using chiral ligands or to the use of chiral auxiliaries are now possible using relatively small organic molecules that can be used in catalytic amounts. Examples of organocatalysis include aminocatalysis,[1,2] (thio)urea-based hydrogen bonding catalysis,[3-5] *N*-heterocyclic carbene-based catalysis,[6,7] and chiral phosphoric acid catalysis.[8-10] Of these, aminocatalysis is one of the most versatile.[11-17]

The simplest asymmetric aminocatalyst employed for this purpose is L-proline, which has been used as a catalyst in both intramolecular and intermolecular asymmetric aldol reactions.[18,19] These reactions proceed through a hydrogen-bound intermediate involving the carboxylic acid group of L-proline[20] (Figure 1a). However, in reactions where the intermediate is unable to form a similar hydrogen-bound intermediate, the enantioselectivity of L-proline is generally poor.[21-24] To alleviate this, L-proline has been modified to diarylprolinol catalysts with large aryl groups, inducing enantioselectivity by steric hindrance of one of the prochiral sides of the enamine/iminium intermediate (Figure 1b).[22,25-27] The diarylprolinol catalysts exhibited a relatively high degree of enantioselectivity. However, the activity of these catalysts is low due to the formation of hemiaminals, which act as resting states during catalysis (Figure 1b). Therefore, the hydroxyl group of the diarylprolinol catalysts was protected with a trimethylsilyl group (Figure 1c). Catalysts of this type, known as Hayashi-Jørgensen catalysts, exhibit high activity and good enantioselectivity.[28-30] In conjunction with the MacMillan imidazolidone-based catalysts,[31-33] these catalysts are prevalent in contemporary enantioselective aminocatalysis.

Cai *et al.*[34] utilized enantioselective aminocatalysis in the enantioselective dipolar [3 + 2] cycloaddition of nitrones to propargylic aldehydes, yielding chiral 4-isoxazolines (Scheme 1). L-Proline and an imidazolidinone catalyst proved ineffective for this transformation. However, a yield of 92% and an enantiomeric excess of 95% were achieved using bis[3,5-bis(trifluoromethyl)phenyl]prolinol (**P2**) as a catalyst. The strongly acidic 3,5-dinitrobenzoic acid was also necessary to maintain high yield and enantioselectivity.

*e-mail: j.roithova@science.ru.nl
Editor handled this article: Emílio Carlos de Lucca Júnior (Guest)
This publication is part of the special issue "Organic Synthesis - BMOS"

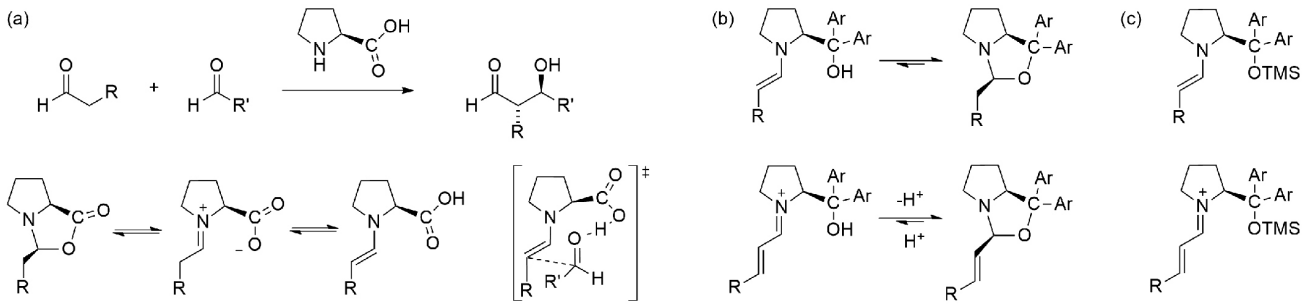

Figure 1. (a) Proline-catalyzed aldol reaction; equilibrium among iminium and enamine intermediates; transition structure for aldol condensation;[20] (b) enamine and iminium ion formed with diarylprolinol catalysts and their transformation to hemiaminals, and (c) enamine and iminium ion with Hayashi-Jørgensen catalysts.[28]

In contrast, silylated catalysts like diphenylprolinol trimethylsilyl ether (**P3**) did not yield any product. This observation contradicts the prevailing trend in organocatalysis, in which silyl-protected catalysts exhibit higher activity than their unprotected analogues. Although the mechanism proposed in the original paper can explain the observed enantioselectivity, the complete lack of reactivity of the TMS-protected catalysts remains unexplained.

Here, the reaction of phenylpropargylaldehyde **1** with *C*-phenyl-*N*-benzylnitrone, hereafter referred to as a nitrone, catalyzed by three distinct diarylprolinol catalysts (**P1-P3**) to yield 4-isoxazoline **4** (Scheme 1) was studied. Our group show that the previously proposed mechanism is incomplete and that additional intermediates and side products play an important role in explaining the observed reactivity. This research was accomplished using a combination of nuclear magnetic resonance (NMR) spectroscopy, electrospray ionization mass spectrometry (ESI-MS), and infrared photodissociation spectroscopy (IRPD).[35,36]

Results

NMR experiments

The formation of iminium ions from catalysts **P1-P3** and aldehyde **1** was studied by ^{1}H NMR. The prolinol catalysts with free hydroxyl group, **P1** and **P2**, formed hemiaminal intermediates (Scheme 2). The hemiaminals could be assigned based on their characteristic signals around 5.2-5.8 ppm (Figures S1-S6, in the Supplementary Information (SI) section).[37-39] Comparing the integrals of the hemiaminal signals with the signal of aldehyde **1** at 9.42 ppm reveals that both catalysts, **P1** and **P2**, react quantitatively with **1** and completely transform to the hemiaminals.

Catalyst **P1** formed only one hemiaminal (signal at 5.28 ppm), which could be assigned to the *syn*-hemiaminal based on nuclear Overhauser effect spectroscopy (NOESY, Figure S2, in the SI section). This diastereoisomer originates from the *E*-isomer of iminium ion **2**$^{+}$. In contrast, catalyst **P2** forms both *syn*- and *anti*-hemiaminals (signals at 5.31 and 5.74 ppm, respectively; Figures S3-S6, in the SI section). The ratio of these signal changes from 1:0.17 in a freshly prepared sample to 1:2 in a 3-day-old sample (Figures S3-S5, in the SI section).

The changing ratio clearly indicates that the formation of the hemiaminal is reversible. The iminium ions have *E*- and *Z*-isomers, which can interconvert due to the conjugation of the π-bonds (see Scheme 2). The *Z*-conformer is energetically disfavored due to the steric repulsion between the alkynyl group and the bulky substituents of the prolinol. However, the closure of the hemiaminal starting from the *Z*-iminium leads to the anti-hemiaminal, which will be energetically favored over the *syn*-isomer and most likely serves as a thermodynamic sink. As a consequence, its formation prevails after a long reaction time.

Initially, no reaction was observed for catalyst **P3** (Figure S7, in the SI section). New signals appeared only after the addition of benzoic acid, which was expected to accelerate iminium ion formation (Figure S8, in the SI

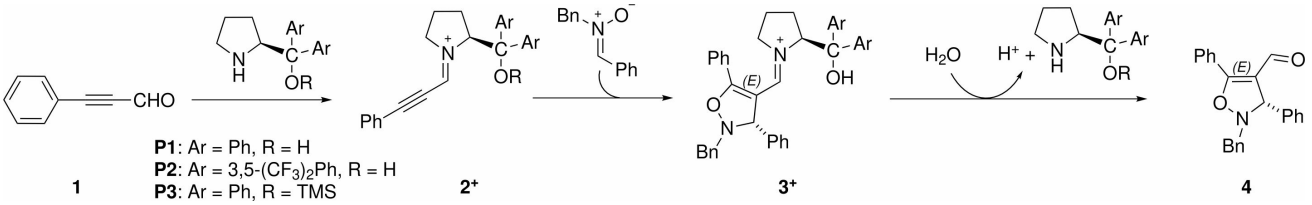

Scheme 1. Enantioselective [3 + 2] cycloaddition catalyzed by diarylprolinol catalysts as reported by Cai *et al.*[34] **P1-P3** are the catalysts used in this study; Ar = aryl group, TMS = trimethylsilyl, Ph = phenyl, Bn = benzyl.

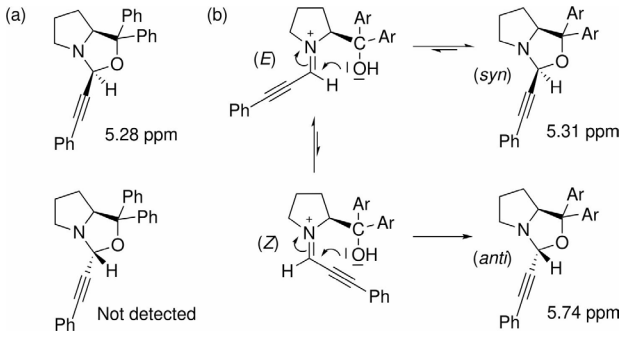

Scheme 2. The hemiaminals ($\mathbf{2}_{off}$) formed from aldehyde **1** with catalysts (a) **P1** and (b) **P2**, Ar = 3,5-$(CF_3)_2$Ph. The chemical shift of the characteristic hemiaminal proton and the suggested equilibria detected in the system with **P2** are indicated.

section). The new signals at 9.74 ppm and around 6.3 ppm are consistent with the formation of singly unsaturated aldehydes, which indicates that aldehyde **1** has undergone an addition to the triple bond. Total correlation spectroscopy (TOCSY) experiments demonstrated that these signals originate from two distinct products (Figures S9-S11, in the SI section). The identities of these compounds were not immediately apparent; therefore, our group proceeded to ESI-MS analysis to obtain further insights into the reactions of prolinol catalysts **P1-P3** with aldehyde **1**.

ESI-MS and IRPD experiments

The ESI-MS spectra of mixtures containing aldehyde **1**, nitrone, 3,5-dinitrobenzoic acid, and catalysts **P1** or **P2** show intermediates $\mathbf{2}^+$ and $\mathbf{3}^+$, alongside protonated catalysts (Figures 2a and 2b). Iminium ions $\mathbf{2}^+$ and $\mathbf{3}^+$ and their protonated hemiaminal forms have identical *m/z* values. To determine which ions are detected by ESI-MS, infrared photodissociation (IRPD) spectra of the mass-selected ions using the helium-tagging technique (Figures 2c and S21(SI section)) were measured. The helium-tagging IRPD technique relies on trapping mass-selected ions in a cryogenic trap.[36] The ions are cooled to the ground vibrational state, where they form complexes with helium atoms (helium-tagged ions). IR photons irradiate the ions. Absorption at a given wavenumber results in a depletion of the number of helium-tagged ions (helium dissociates due to the increase in the internal energy of the absorbing ion). For more information, see SI.

The IRPD spectrum of the adduct between **P1** and **1** (*m/z* 366) clearly reveals an O–H vibration at 3660 cm^{-1}. The free hydroxyl attests to the iminium form of these ions in the gas phase. Also, all bands identified at the fingerprint region are consistent with the iminium structure of the gaseous ions (see Figure 2c). Most likely, the protonation of the hemiaminal present in the solution occurs at the oxygen atom, leading to the ring opening and regeneration of the iminium ion. The IRPD spectrum of intermediate $\mathbf{3}^+$ shows an analogous O–H vibration, also suggesting that the ions have the iminium form in the gas phase (Figure S21, in the SI section). Density functional theory (DFT) calculations suggest that the iminium forms $\mathbf{2}^+$ and $\mathbf{3}^+$ are by 16.9 and 20.4 kcal mol^{-1} more stable than the alternative protonated hemiaminal forms in the gas phase. Note that with the ESI-MS method, we study hemiaminals (characterized as neutral species by ^{1}H NMR in the solution) that get protonated during the ionization process. The protonation

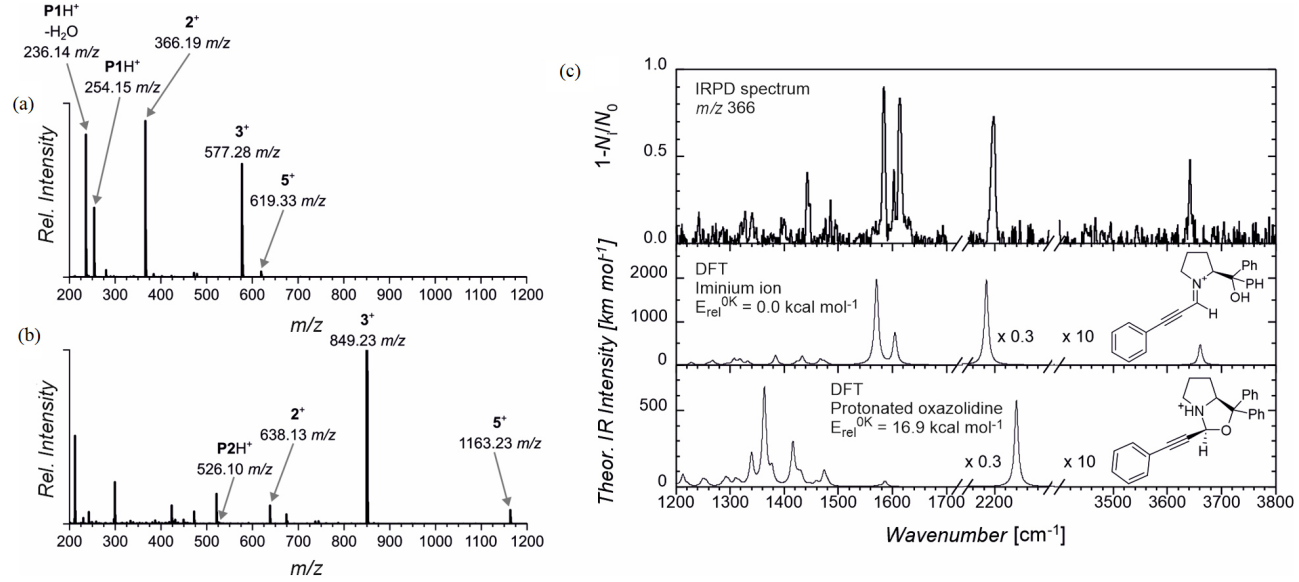

Figure 2. ESI-MS spectra of solutions containing (a) **P1** and (b) **P2**; each spectrum is shown after 20 min of reaction time at 25 °C with 0.2 mM catalyst, 0.5 mM aldehyde **1**, 5 mM nitrone, and 0.2 mM 3,5-dinitrobenzoic acid in chloroform, and (c) IRPD spectrum of the mass-selected ions $\mathbf{2}^+$ formed from catalyst **P1** and a comparison with the theoretical IR spectra of possible iminium and protonated oxazole isomers.

at the oxygen atom of the hemiaminal is energetically favored, leading to the opening of the oxazolidine ring. The calculations are performed in the gas phase because they refer to isolated ions. Nevertheless, deprotonation and protonation at the oxygen atom are also mechanisms by which the equilibrium between the iminium and oxazolidine forms in the solution is established.

The ESI-MS spectrum of the reaction mixture of aldehyde **1**, nitrone, and catalyst **P3** shows iminium intermediates $\mathbf{2}^+$ (*m/z* 428.22) and $\mathbf{3}^+$ (*m/z* 649.32), alongside protonated catalyst (*m/z* 326.19) and degraded catalyst (*m/z* 236.14) (Figure 3a). In addition, ion $\mathbf{6}^+$ (*m/z* 763.41) was detected and corresponds to an adduct of intermediate $\mathbf{2}^+$ with another molecule of catalyst **P3**. ESI-MS analysis of the NMR sample with an unknown addition product of **1** (see above) showed that the ions with *m/z* 763.41 are the dominant ions in the spectrum (Figure S12, in the SI section). Importantly, analogous but less abundant ions were also detected in reactions catalyzed by **P1** and **P2** (*m/z* 619.33 and 1163.23 in Figure 2, respectively). Hence, it indicates that the detected ions $\mathbf{6}^+$ are associated with an undesired side-reaction pathway, which is minor in reactions catalyzed by **P1** and **P2**, but becomes the major pathway in the reaction catalyzed by **P3**.

The nucleophilic addition of a proline to the iminium intermediate $\mathbf{2}^+$ initially leads to an allene (**5**), which can be protonated to yield detected $\mathbf{6}^+$ (Figure 3b). The ions $\mathbf{6}^+$ have an amine and an iminium in conjugation with two mesomeric forms $\mathbf{6a}^+$ and $\mathbf{6b}^+$. Because of the conjugation, the ions can isomerize at the double bonds, leading to different possible combinations of configurations at the double bonds. To confirm the structure of the detected ions $\mathbf{6}^+$, we investigated the mass-selected ions (*m/z* 763.41) by helium-tagging IRPD spectroscopy (Figure 3c). The experimental spectrum closely matches the theoretically predicted IR spectrum of the vinamidinium product formed by nucleophilic attack by catalyst **P3** at the β-position of iminium ion $\mathbf{2}^+$.[40,41]

Assuming the hydrolysis of the mesomeric forms $\mathbf{6a}^+$ and $\mathbf{6b}^+$, the final products enaminone **7a** and enaminal **7b** can form (Figure 3b). These structures are consistent with the two molecules detected in the ^{1}H NMR spectrum of the acidified reaction mixture (Figure S11, in the SI section).[42-45] This type of reactivity is documented in the literature for similar propargylic iminium ions and is thought to involve allenamine intermediates (Figure 3b).[46-49]

Discussion

In this study, the seemingly paradoxical reactivity of prolinol and prolinol silyl ether catalysts in the [3 + 2] cycloaddition of *C*-phenyl-*N*-benzylnitrone to phenylpropargylaldehyde was investigated, in which usually sluggish prolinol catalysts yielded the product, whereas the optimized prolinol silyl ether catalysts failed to mediate the desired reaction.

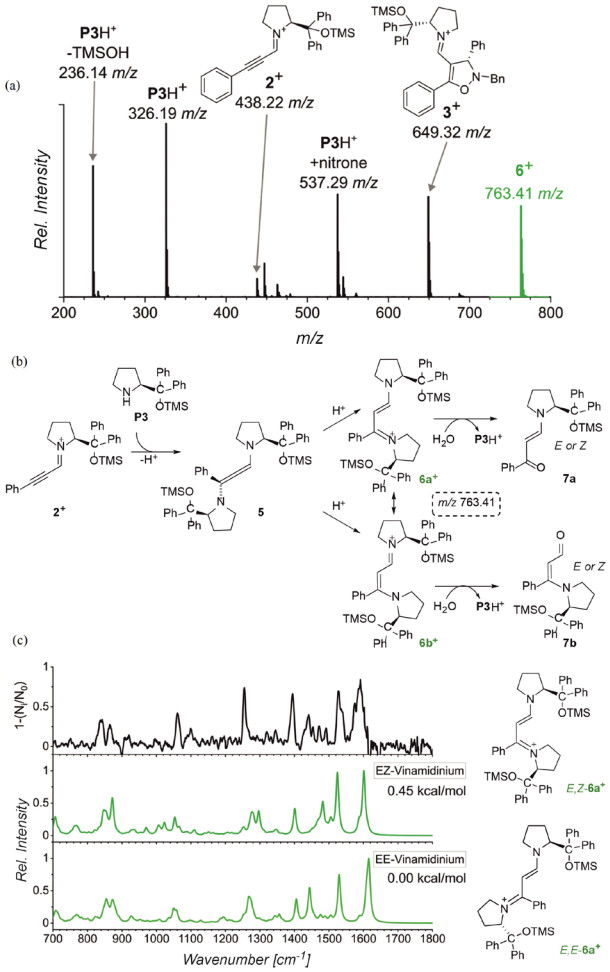

Figure 3. (a) ESI-MS spectrum of a reaction mixture containing 0.5 mM aldehyde **1**, 0.2 mM catalyst **P3**, and 5 mM nitrone in chloroform after 20 min of reaction time at 25 °C. Catalyst **P3** and its fragments and adducts are indicated, along with intermediates $\mathbf{2}^+$, $\mathbf{3}^+$, and ions $\mathbf{6}^+$; (b) the side reaction proceeds via the conjugated iminium ions, followed by the hydrolysis to either enaminone or enaminal. Not all possible isomers are shown, and (c) IRPD spectrum of ions $\mathbf{6}^+$ (*m/z* 763.41) compared to the theoretical spectra of the EZ- and EE-isomers of the vinamidinium ions $\mathbf{6}^+$, as calculated at B3LYP-GD3BJ/6-311+G(2d,p) (scaling factor 0.98). Other potential isomers and rotamers of the vinamidinium ion are omitted.

The NMR experiments demonstrated that iminium ion $\mathbf{2}^+$ reacts intramolecularly to form hemiaminal $\mathbf{2}_{\mathbf{off}}$ in the reactions of both catalysts **P1** and **P2**, with nearly all of the catalyst incorporated into $\mathbf{2}_{\mathbf{off}}$ under our experimental conditions. With time, the kinetically preferred *syn*-hemiaminal rearranged to the *anti*-form, indicating an equilibrium between $\mathbf{2}_{\mathbf{off}}$ and $\mathbf{2}^+$.[52] Consequently, the equilibrium concentration of iminium $\mathbf{2}^+$ provides the opportunity for the desired cycloaddition reaction with the nitrone reactant (blue catalytic cycle in Figure 4).

In the reaction of catalyst **P3** with aldehyde **1**, no hemiaminal can form due to the trimethylsilyl protection of the hydroxyl group. The initially formed iminium ions $\mathbf{2}^+$ react either by cycloaddition with a nitrone to form $\mathbf{3}^+$, or with another proline catalyst, **P3**, to form the allene intermediate **5**. Protonation of allene **5** yields the detected ions $\mathbf{6}^+$, which can exist in several isomeric forms. Upon acidification, $\mathbf{6}^+$ intermediates hydrolyze to enaminone (**7a**) or enaminal (**7b**) products with **P3** incorporated into the structure. The corresponding enaminals and enaminones are the only products observed by ^{1}H NMR spectroscopy. Therefore, the addition of **P3** to $\mathbf{2}^+$ is faster than that of the nitrone. Consequently, the reaction sequence towards **7a** and **7b** leads to complete catalyst depletion, and the desired cycloaddition product is not formed (red catalytic cycle in Figure 4).

Hence, the *quasi*-quantitative formation of hemiaminal $\mathbf{2}_{\mathbf{off}}$ in the cycloaddition reaction catalyzed by **P1** or **P2** is essential. The formation of off-cycle intermediate $\mathbf{2}_{\mathbf{off}}$ removes free prolinol molecules **P1** and **P3** from the solution, and, therefore, these molecules are not available to make a nucleophilic attack at the iminium ion $\mathbf{2}^+$. Hence, the red catalytic cycle, leading to $\mathbf{6a}^+/\mathbf{6b}^+$ and ultimately to **7a** and **7b**, is suppressed (Figure 4). The intermediates and products are still observed but are minor due to the negligible concentration of free prolinol (**P1** or **P2**). Instead, sequestering **P1** and **P3** in the off-cycle intermediate $\mathbf{2}_{\mathbf{off}}$ makes the way to the slower reaction between the transiently formed iminium ions $\mathbf{2}^+$ and the nitrone reactant (blue catalytic cycle in Figure 4). This reaction mechanism provides another example of the important role of an off-cycle intermediate, which enables, rather than hinders, the desired reactivity.[53]

For additional references consult indicated literature.[54-57]

Conclusions

In this study, a combination of NMR, ESI-MS, and IRPD experiments was utilized to elucidate the differing outcomes of the organocatalytic nitrone cycloaddition, when catalyzed by different prolinol-derived catalysts. Our group showed that iminium ion $\mathbf{2}^+$ formed by condensation of a propargyl aldehyde and prolinol can rapidly react with another prolinol to form vinamidinium intermediates $\mathbf{6}^+$. The addition of an acid leads to the formation of enaminone (**7a**) and enaminal (**7b**) side productss, each incorporating one molecule of the prolinol catalyst.

The outcome of the catalysis depends on the structure of the prolinol-derived catalyst. If the catalyst has a silylated hydroxyl group (such as **P3**), then the undesired side pathway rapidly depletes the catalyst of the reaction mixture, and the desired cycloaddition reaction is not observed. If the catalyst has a free hydroxyl group (such as **P1** and **P2**), initially formed iminium ion $\mathbf{2}^+$ can cyclize to the unreactive hemiaminal form $\mathbf{2}_{\mathbf{off}}$. While this off-cycle equilibrium reaction is usually undesired, as it slows the desired transformation, in this reaction, it sequesters the catalysts from the reaction mixture, allowing the transiently formed $\mathbf{2}^+$ to react with the nitrone.

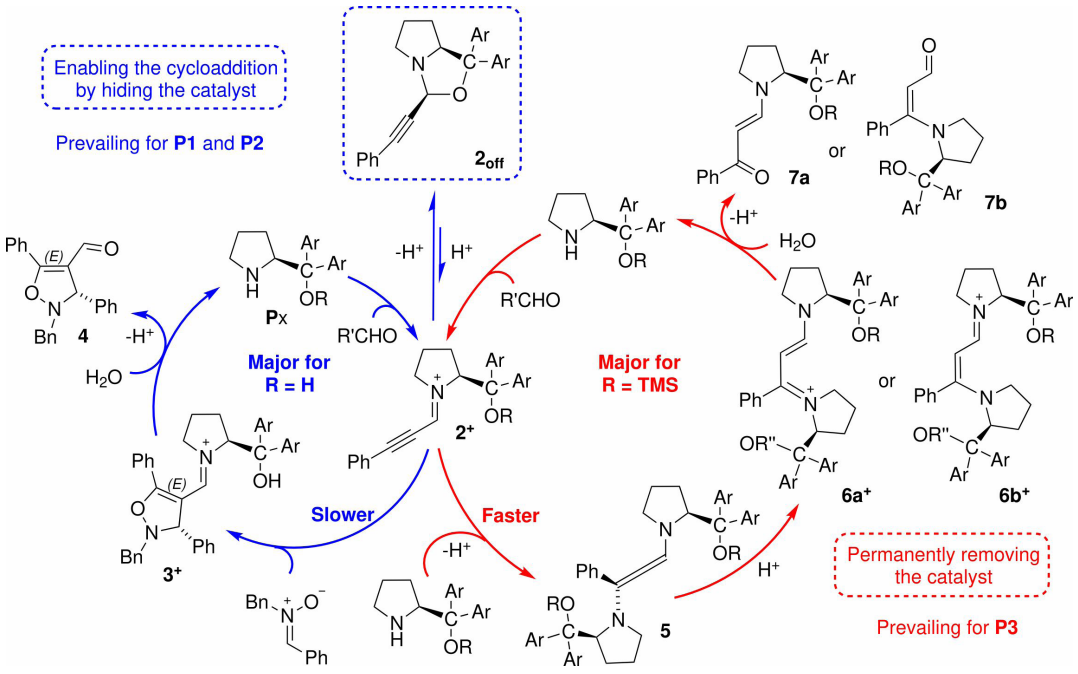

Figure 4. Competing reactions in the nitrone addition to alkynes catalysed by prolinol catalysts; R'CHO = phenylpropargyl aldehyde.

The expanded mechanism proposed in this study has implications for other organocatalytic reactions involving propargyliminium ions, in which the desired reaction step involving this ion is slow (e.g., cycloadditions with large entropic barriers) and may be outcompeted by simple conjugated additions. The efficiency of such reactions may be improved by switching to unprotected prolinol catalysts, thereby expanding the scope of organocatalytic reactions involving propargylaldehydes.

Experimental

NMR experiments

NMR experiments were conducted on a Bruker Avance III 400 MHz spectrometer. The residual solvent peak of chloroform (δ_H 7.26 ppm) was used to reference the spectra. The NMR yield was determined by preparing a sample in chloroform-d containing 0.2 M phenylpropargylaldehyde, 0.24 M *C*-phenyl-*N*-benzylnitrone, 40 mM catalyst (**P1** or **P2**), and 40 mM (3,5-dinitro)benzoic acid if present. 1,3,5-Trimethoxybenzene at a concentration of 0.2 M was used as an internal standard. Each sample was allowed to react at 25 °C and was measured several times over the course of 96 h. The aldehyde signal at 9.80 ppm of the product 4-isoxazoline and the aromatic signal at 6.10 ppm of the internal standard were used to determine the yield over time. NOESY experiments to determine hemiaminal configurations were performed on samples containing 150 mM phenylpropargylaldehyde and 30 mM aldehyde (**P1**-**P2**) in chloroform-*d*. TOCSY experiments to identify the decomposition products from catalyst **P3** were performed on a Bruker Avance III 500 MHz spectrometer equipped with a Prodigy BB cryoprobe. A sample containing 200 mM phenylpropargylaldehyde, 40 mM catalyst **P3**, and 40 mM benzoic acid in chloroform-*d* was prepared. The sample was cooled to 10 °C to resolve the signals better.

ESI-TIMS-TOF-MS experiments

Trapped ion mobility spectrometry-mass spectrometry experiments were performed on a TIMS-TOF-MS (Bruker Daltonics). Ions were generated by electrospray ionization (ESI), with the following settings: capillary voltage 5 kV, end plate offset 50 V, dry gas 3.0 L min^{-1}, dry temperature 300 °C and nebulizer gas 0.0 bar. TIMS was operated in custom mode at a range of 0.65-1.26 V s cm^{-2} with a ramp time of 950 ms and an accumulation time of 10 ms. Radiofrequency (RF) funnel 1 was operated at 400 Vpp and RF funnel 2 at 200 Vpp, while the multipole radiofrequency was set to 500 Vpp and the deflection delta voltage to 70 V. The quadrupole ion energy was set to 8 eV, while the transfer time and pre-pulse storage time were set to 55 and 5 µs, respectively. Though mobilograms were recorded for most spectra, they could not be conclusively assigned to the isomers of ions $\mathbf{2}^+$ and $\mathbf{3}^+$. The mobilograms were therefore not used in this research.

IRPD experiments

He-tagging infrared photodissociation experiments were performed by spraying the reaction mixture using the ESI source of the ISORI instrument, described in detail elsewhere.[35] The ions of interest were mass-selected and trapped using helium buffer gas in a cryogenic trap at a temperature of 3.5 K. The cooled ions formed helium-tagged complexes (N_{i0}). Using IR OPO/OPA (optical parametric oscillator and amplifier) photon source, the ions were irradiated (1 or 2 s) and the surviving helium complexes counted ($N_i(\nu)$). The pulse sequence was repeated with the IR beam alternately admitted or blocked over the desired IR range (see details in Figure S19, in the SI section). The $N_i(\nu)/N_{i0}$ ratio relates to the helium complex depletion due to the absorption of IR photons at a given wavenumber (ν).

DFT calculations

DFT calculations were performed using the Gaussian 16 C.01 software package.[58] All calculations were carried out at the B3LYP/6-311+G(2d,p) level of theory with empirical dispersion version GD3BJ.[59] The B3LYP functional was selected because it provides theoretical IR spectra that are usually in very good agreement with experimental data.[60] The harmonic IR spectra were scaled by 0.96. All calculations were performed in the gas phase, and the reported structures were fully minimized. The frequency calculations were performed to confirm the absence of imaginary frequencies and to obtain the relevant IR spectra. The reported energies refer to 0 K (including zero-point vibrational energy). The starting geometries were obtained after the initial conformational search. However, we did not perform the full conformational search using molecular dynamics. The IR spectra show a very good agreement with the experiments.

Supplementary Information

Supplementary Information (experimental details and further experimental results) are available free of charge at http://jbcs.sbq.org.br as a PDF file.

Data Availability Statement

All experimental data and the results of calculations are freely available at https://doi.org/10.34973/e5jc-5h44.

Acknowledgments

The authors would like to thank the Netherlands Organization for Scientific Research for providing the necessary funding (VI.C.192.044).

Author Contributions

M. A. H. was responsible for conceptualization, data curation, formal analysis, investigation, writing – original draft; A. Y. P. for formal analysis, investigation, writing – review & editing; J. R. for conceptualization, investigation, funding acquisition, methodology, supervision, writing – review & editing.

References

1. Melchiorre, P.; Marigo, M.; Carlone, A.; Bartoli, G.; *Angew. Chem., Int. Ed.* **2008**, *47*, 6138. [Crossref]
2. List, B.; *Synlett* **2001**, *2001*, 1675. [Crossref]
3. Li, Q.-H.; Zhang, G.-S.; Wang, Y.-H.; Mei, M.-S.; Wang, X.; Liu, Q.; Yang, X.-D.; Tian, P.; Lin, G.-Q.; *Org. Chem. Front.* **2019**, *6*, 2624. [Crossref]
4. Takemoto, Y.; *Chem. Pharm. Bull.* **2010**, *58*, 593. [Crossref]
5. Reisman, S. E.; Doyle, A. G.; Jacobsen, E. N.; *J. Am. Chem. Soc.* **2008**, *130*, 7198. [Crossref]
6. Chakraborty, S.; Barik, S.; Biju, A. T.; *Chem. Soc. Rev.* **2025**, *54*, 1102. [Crossref]
7. Singha, S.; Patra, T.; Daniliuc, C. G.; Glorius, F.; *J. Am. Chem. Soc.* **2018**, *140*, 3551. [Crossref]
8. Maji, R.; Mallojjala, S. C.; Wheeler, S. E.; *Chem. Soc. Rev.* **2018**, *47*, 1142. [Crossref]
9. Da, B.-C.; Xiang, S.-H.; Li, S.; Tan, B.; *Chin. J. Chem.* **2021**, *39*, 1787. [Crossref]
10. Shao, Y.-D.; Cheng, D.-J.; *ChemCatChem* **2021**, *13*, 1271. [Crossref]
11. Faghtmann, J.; Andresen, S. S. P.; Østergaard, A. R.; Jørgensen, K. A.; *Chem. - Eur. J.* **2025**, *31*, e202403656. [Crossref]
12. Guo, C.-S.; Du, Y.-H.; Huang, Z.-Z.; *Chem. Commun.* **2011**, *47*, 3995. [Crossref]
13. Jessen, N. I.; Bura, M.; Bertuzzi, G.; Jørgensen, K. A.; *Angew. Chem., Int. Ed.* **2021**, *60*, 18527. [Crossref]
14. Corti, V.; Barløse, C. L.; Østergaard, N. L.; Kristensen, A.; Jessen, N. I.; Jørgensen, K. A.; *J. Am. Chem. Soc.* **2023**, *145*, 1448. [Crossref]
15. Vicario, J.; *Synlett* **2016**, *27*, 1006. [Crossref]
16. Rigotti, T.; Mas-Ballesté, R.; Alemán, J.; *ACS Catal.* **2020**, *10*, 5335. [Crossref]
17. Del Vecchio, A.; Sinibaldi, A.; Nori, V.; Giorgianni, G.; Di Carmine, G.; Pesciaioli, F.; *Chem. - Eur. J.* **2022**, *28*, e202200818. [Crossref]
18. Northrup, A. B.; MacMillan, D. W. C.; *J. Am. Chem. Soc.* **2002**, *124*, 6798. [Crossref]
19. Hajos, Z. G.; Parrish, D. R.; *J. Org. Chem.* **1974**, *39*, 1615. [Crossref]
20. Allemann, Ch.; Gordillo, R.; Clemente, F. R.; Cheong, P. H. Y.; Houk, K. N.; *Acc. Chem. Res.* **2004**, *37*, 558. [Crossref]
21. Marigo, M.; Fielenbach, D.; Braunton, A.; Kjærsgaard, A.; Jørgensen, K. A.; *Angew. Chem., Int. Ed.* **2005**, *44*, 3703. [Crossref]
22. Marigo, M.; Wabnitz, T. C.; Fielenbach, D.; Jørgensen, K. A.; *Angew. Chem., Int. Ed.* **2005**, *44*, 794. [Crossref]
23. Zhong, C.; Chen, Y.; Petersen, J. L.; Akhmedov, N. G.; Shi, X.; *Angew. Chem., Int. Ed.* **2009**, *48*, 1279. [Crossref]
24. Hayashi, Y.; Gotoh, H.; Hayashi, T.; Shoji, M.; *Angew. Chem., Int. Ed.* **2005**, *44*, 4212. [Crossref]
25. Halland, N.; Braunton, A.; Bachmann, S.; Marigo, M.; Jørgensen, K. A.; *J. Am. Chem. Soc.* **2004**, *126*, 4790. [Crossref]
26. Juhl, K.; Jørgensen, K. A.; *Angew. Chem.* **2003**, *115*, 1536. [Crossref]
27. Melchiorre, P.; Jørgensen, K. A.; *J. Org. Chem.* **2003**, *68*, 4151. [Crossref]
28. Jensen, K. L.; Dickmeiss, G.; Jiang, H.; Albrecht, Ł.; Jørgensen, K. A.; *Acc. Chem. Res.* **2012**, *45*, 248. [Crossref]
29. Franzén, J.; Marigo, M.; Fielenbach, D.; Wabnitz, T. C.; Kjærsgaard, A.; Jørgensen, K. A.; *J. Am. Chem. Soc.* **2005**, *127*, 18296. [Crossref]
30. Donslund, B. S.; Johansen, T. K.; Poulsen, P. H.; Halskov, K. S.; Jørgensen, K. A.; *Angew. Chem., Int. Ed.* **2015**, *54*, 13860. [Crossref]
31. Jen, W. S.; Wiener, J. J. M.; MacMillan, D. W. C.; *J. Am. Chem. Soc.* **2000**, *122*, 9874. [Crossref]
32. Ahrendt, K. A.; Borths, C. J.; MacMillan, D. W. C.; *J. Am. Chem. Soc.* **2000**, *122*, 4243. [Crossref]
33. Beeson, T. D.; MacMillan, D. W. C.; *J. Am. Chem. Soc.* **2005**, *127*, 8826. [Crossref]
34. Cai, X.; Wang, C.; Sun, J.; *Adv. Synth. Catal.* **2012**, *354*, 359. [Crossref]
35. Jašík, J.; Žabka, J.; Roithová, J.; Gerlich, D.; *Int. J. Mass Spectrom.* **2013**, *354-355*, 204. [Crossref]
36. Roithová, J.; Gray, A.; Andris, E.; Jašík, J.; Gerlich, D.; *Acc. Chem. Res.* **2016**, *49*, 223. [Crossref]
37. Hayashi, Y.; Nagai, K.; Umemiya, S.; *Chem. Asian J.* **2019**, *14*, 4146. [Crossref]
38. Periasamy, M.; Sanjeevakumar, N.; Dalai, M.; Gurubrahamam, R.; Reddy, P. O.; *Org. Lett.* **2012**, *14*, 2932. [Crossref]

39. Macharia, J.; Wambua, V.; Hong, Y.; Harris, L.; Hirschi, J. S.; Evans, G. B.; Vetticatt, M. J.; *Angew. Chem., Int. Ed.* **2017**, *56*, 8756. [Crossref]
40. Davies, I. W.; Marcoux, J.-F.; Wu, J.; Palucki, M.; Corley, E. G.; Robbins, M. A.; Tsou, N.; Ball, R. G.; Dormer, P.; Larsen, R. D.; Reider, P. J.; *J. Org. Chem.* **2000**, *65*, 4571. [Crossref]
41. Lloyd, D.; McNab, H.; *Angew. Chem., Int. Ed. Engl.* **1976**, *15*, 459. [Crossref]
42. Nikolai, J.; Taubmann, G.; Maas, G.; *Z. Naturforsch. B* **2003**, *58*, 217. [Crossref]
43. Jin, X.; Yamaguchi, K.; Mizuno, N.; *Angew. Chem., Int. Ed.* **2014**, *53*, 455. [Crossref]
44. Schuppe, A. W.; Cabrera, J. M.; McGeoch, C. L. B.; Newhouse, T. R.; *Tetrahedron* **2017**, *73*, 3643. [Crossref]
45. Kang, Y.-W.; Cho, Y. J.; Han, S. J.; Jang, H.-Y.; *Org. Lett.* **2016**, *18*, 272. [Crossref]
46. Alemán, J.; Alvarado, C.; Marcos, V.; Núñez, A.; García Ruano, J.; *Synthesis* **2011**, *2011*, 1840. [Crossref]
47. Liu, C.; Zhang, X.; Wang, R.; Wang, W.; *Org. Lett.* **2010**, *12*, 4948. [Crossref]
48. Lee, Y.; Heo, S.; Kim, S.-G.; *Adv. Synth. Catal.* **2015**, *357*, 1545. [Crossref]
49. Zhang, J.; Xu, Y.; Wang, Z.; Zhong, R.; Wang, Y.; *J. Org. Chem.* **2021**, *86*, 4262. [Crossref]
50. Jašíková, L.; Anania, M.; Hybelbauerová, S.; Roithová, J.; *J. Am. Chem. Soc.* **2015**, *137*, 13647. [Crossref]
51. Hilgers, R.; Yong Teng, S.; Briš, A.; Pereverzev, A. Y.; White, P.; Jansen, J. J.; Roithová, J.; *Angew. Chem., Int. Ed.* **2022**, *61*, e202205720. [Crossref]
52. Schmid, M. B.; Zeitler, K.; Gschwind, R. M.; *J. Am. Chem. Soc.* **2011**, *133*, 7065. [Crossref]
53. Burés, J.; Armstrong, A.; Blackmond, D. G.; *J. Am. Chem. Soc.* **2011**, *133*, 8822. [Crossref]
54. Frisch, M. J.; Trucks, G. W.; Schlegel, H. B.; Scuseria, G. E.; Robb, M. A.; Cheeseman, J. R.; Scalmani, G.; Barone, V.; Petersson, G. A.; Nakatsuji, H.; Li, X.; Caricato, M.; Marenich, A. V.; Bloino, J.; Janesko, B. G.; Gomperts, R.; Mennucci, B.; Hratchian, H. P.; Ortiz, J. V.; Izmaylov, A. F.; Sonnenberg, J. L.; Williams-Young, D.; Ding, F.; Lipparini, F.; Egidi, F.; Goings, J.; Peng, B.; Petrone, A.; Henderson, T.; Ranasinghe, D.; Zakrzewski, V. G.; Gao, J.; Rega, N.; Zheng, G.; Liang, W.; Hada, M.; Ehara, M.; Toyota, K.; Fukuda, R.; Hasegawa, J.; Ishida, M.; Nakajima, T.; Honda, Y.; Kitao, O.; Nakai, H.; Vreven, T.; Throssell, K.; Montgomery Jr., J. A.; Peralta, J. E.; Ogliaro, F.; Bearpark, M. J.; Heyd, J. J.; Brothers, E. N.; Kudin, K. N.; Staroverov, V. N.; Keith, T. A.; Kobayashi, R.; Normand, J.; Raghavachari, K.; Rendell, A. P.; Burant, J. C.; Iyengar, S. S.; Tomasi, J.; Cossi, M.; Millam, J. M.; Klene, M.; Adamo, C.; Cammi, R.; Ochterski, J. W.; Martin, R. L.; Morokuma, K.; Farkas, O.; Foresman, J. B.; Fox, D. J.; *Gaussian 16*, *Revision A.03*, Inc.: Wallingford, CT, USA, 2016.
55. Grimme, S.; Antony, J.; Ehrlich, S.; Krieg, H.; *J. Chem. Phys.* **2010**, *132*, 154104. [Crossref]
56. Pracht, P.; Grant, D. F.; Grimme, S.; *J. Chem. Theor. Comp.* **2020**, *16*, 7044. [Crossref]
57. Bairagi, A.; Pereverzev, A. Y.; Tinnemans, P.; Pidko, E. A.; Roithová, J.; *J. Am. Chem. Soc.* **2024**, *146*, 5480. [Crossref]
58. Alemán, J.; Fraile, A.; Marzo, L.; Ruano, J. L. G.; Izquierdo, C.; Díaz-Tendero, S.; *Adv. Synth. Catal.* **2012**, *354*, 1665. [Crossref]
59. Arakawa, Y.; Ueta, S.; Okamoto, T.; Minagawa, K.; Imada, Y.; *Synlett* **2020**, *31*, 866. [Crossref]
60. Kocsis, L. S.; Kagalwala, H. N.; Mutto, S.; Godugu, B.; Bernhard, S.; Tantillo, D. J.; Brummond, K. M.; *J. Org. Chem.* **2015**, *80*, 11686. [Crossref]

Submitted: April 24, 2026
Final version online: June 11, 2026